https://doi.org/10.1016/j.ultras.2021.106578

Surface/sub-surface Crack-scattered Nonlinear Rayleigh Waves: A Full Analytical Solution based on Elastodynamic Reciprocity Theorem

Lei Xu[a], Kai Wang[b], Yiyin Su[a], Yi He[a], Jianwei Yang[a], Shenfang Yuan[c] and Zhongqing Su[a,d] *

[a] Department of Mechanical Engineering
The Hong Kong Polytechnic University, Kowloon, Hong Kong SAR

[b] Department of Aeronautical and Aviation Engineering
The Hong Kong Polytechnic University, Kowloon, Hong Kong SAR

[c] State Key Lab of Mechanics and Control of Mechanical Structures
Nanjing University of Aeronautics and Astronautics, Nanjing 210016, P.R. China

[d] The Hong Kong Polytechnic University Shenzhen Research Institute
Shenzhen 518057, P.R. China

submitted to ***Ultrasonics***

(first submitted on 1st June 2021; revised and resubmitted on 3rd August 2021; further revised and resubmitted on 9th September 2021)

* To whom correspondence should be addressed. Tel.: +852-2766-7818, Fax: +852-2365-4703;
Email: Zhongqing.Su@polyu.edu.hk (Prof. Zhongqing Su, *Ph.D*)

Abstract

High-order harmonics and sub-harmonics that are engendered upon interaction between surface Rayleigh waves and material flaws have been exploited intensively, for characterizing material defects on or near to waveguide surfaces. Nevertheless, theoretical interpretation on underlying physics of defect-induced nonlinear features of Rayleigh waves remains a daunting task, owing to the difficulty in analytically modeling the stress and displacement fields of a Rayleigh wave in the vicinity of defect, in an explicit and accurate manner. In this study, the Rayleigh wave scattered by a surface or a sub-surface micro-crack is scrutinized analytically, and the second harmonic triggered by the clapping and rubbing behaviors of the micro-crack is investigated, based on the elastodynamic reciprocity theorem. With a virtual wave approach, a full analytical, explicit solution to the micro-crack-induced second harmonic wavefield in the propagating Rayleigh wave is ascertained. Proof-of-concept numerical simulation is performed to verify the analytical solution. Quantitative agreement between analytical and numerical results has demonstrated the accuracy of the solution when used to depict a surface/sub-surface crack-perturbed Rayleigh wavefield and to calibrate the crack-induced wave nonlinearity. The analytical modeling and solution advance the use of Rayleigh waves for early awareness and quantitative characterization of embryonic material defects that are on or near to structural surfaces.

***Keywords*:** Rayleigh waves; second harmonic generation; elastodynamic reciprocity theorem; surface crack; sub-surface crack

1. Introduction

Invisible sub-surface flaws, often ignored in ordinary nondestructive evaluation owing to their close proximity to transducers that are placed on the sample surface, remarkably jeopardize structural integrity and are liable for numerous structural failures. Under a cyclic load, a surface/sub-surface flaw can progress quickly from its embryo to a critical degree without sufficient warning. Aimed at detecting the onset of a surface/sub-surface flaw, a diversity of ultrasonics-driven evaluation approaches has been readily available, making use of various modalities of wave modes including longitudinal waves [1], Rayleigh-Lamb waves [2-5], bulk waves [6-9] and shear horizontal waves [10-12]. In such a context, provided the linear features of ultrasonic waves (*e.g.*, delay in time-of-flight, mode conversion, degree of energy dissipation, reflection and transmission coefficients) are concerned, approaches may not be adequately competent to pinpoint and depict an embryonic flaw, dimensions of which are significantly smaller than the wavelength of the incident wave – that is because a flaw of such dimensions usually does not incur phenomenal wave scattering upon interaction with the incident wave. In contrast, methods making use of nonlinear attributes of ultrasonic waves, such as the high-order harmonics or sub-harmonics generated by the clapping (*a.k.a.*, breathing) and rubbing motions of a micro-crack [13-15] or nonlinear modulation [16, 17], have proven effectiveness in characterizing small-scale flaws, thanks to the superior sensitivity of nonlinear wave features to the microstructural evolution or initial material degradation even at a weak degree.

Contrast to bulk waves that thoroughly disseminate in a waveguide, a Rayleigh wave decays exponentially with depth, and particles in a Rayleigh wave oscillate in an elliptical pattern, with the major axis of the ellipse perpendicular to the surface of the waveguide [18]. It is noteworthy that the Rayleigh wave explored in this study is different from wedge waves or edge waves [19-22] which are guided by the apex of a plate-like waveguide. Wedge waves and edge waves propagate in the vicinity of the structural boundary (*i.e.*, edge of a waveguide) and the wave energy is concentrated near the edge. A Rayleigh wave is guided by a free surface of a waveguide and constrains its major energy to the waveguide surface**.** With the energy dominance near to the waveguide surface, Rayleigh-Lamb waves have been employed to locate [23, 24], orientate [25] and evaluate [26-29] surface or sub-surface flaws. Amongst demonstrated paradigms, the second harmonic generation is one of the wave features that has been exploited extensively. The periodic opening and closing behavior of a crack-like flaw, under a cyclic load or under the modulation of an incident wave (referred to as *clapping* or *breathing* behavior), along with the rubbing motion, can distort propagation of an incident Rayleigh wave, as a consequence of which the high-order harmonics, as typified by the second harmonic, are induced. Good supply of research, in either an analytical or an experimental nature, has investigated and interpreted the crack-scattered waves and second harmonics in Rayleigh-Lamb waves, on which basis a surface or a sub-surface crack can be detected and evaluated [30-34]. Representatively, Lamb waves scattered by a surface-breaking crack in a two-dimensional (2D) elastic waveguide and the accordingly emanated second harmonics were studied by Shen and Giurgiutiu [35], and a damage index was proposed to correlate the acoustic nonlinearity in the captured waves with the crack severity. Wang *et. al.* [13, 25] scrutinized the circumferential pattern of the second harmonic of Lamb waves generated by an inclined fatigue crack and utilized the harmonic magnitude to determine the crack orientation. Yelve *et. al.* [36] explored the first three high-order (*e.g.*, 1st, 2nd and 3rd order) harmonics of a Lamb wave upon interaction with a transverse crack, and defined a spectral index with these harmonics for evaluating the crack depth.

Experimentally, nonlinear Rayleigh waves have been explored by Walker *et. al.* [37], Zeitvogel *et. al.* [38], and Pfeifer *et. al.* [39], respectively, for the purpose of assessing fatigue damage, stress corrosion cracking or damage-induced plasticity in metals. In these experimental studies, the magnitude of surface damage-induced high-order harmonic was observed to augment in a Rayleigh wave, as damage accumulated. Therefore, the severity of surface damage can be assessed by virtue of the intensity of captured high-order harmonic. On the other hand, theoretical or analytical exploration on the interaction of a Rayleigh wave with a clapping surface crack has been fairly limited in a linear domain, focusing on the linear feature changes of a Rayleigh wave caused by a surface or sub-surface crack. To mention but a few, the linear scattering of a Rayleigh wave by a crack was thoroughly examined by Yang and Achenbach [31, 40], Wang *et. al.* [30, 32] and Phan *et.al.* [41], respectively. Instead of using a complicated integral transform, the Rayleigh wave scattered by a crack was formulated in these studies as the radiation from equivalent body forces based on the elastodynamic reciprocity theorem.

However, analytical illustration of the principle and mechanism behind the crack-generated second harmonics of Rayleigh waves is still absent, let alone an explicit, quantitative solution to the magnitude of the crack-induced second harmonics. This is in part owing to the challenge in analytically modeling the stress and displacement fields of a Rayleigh wave in the vicinity of defect, in an explicit and accurate manner. Among trailblazing attempts, Deng *et. al.* [42] interrogated the propagation of a Rayleigh wave in a medium with randomly distributed surface micro-cracks using perturbation analysis and numerical simulation. Thiele *et. al.* [43] also utilized the perturbation approach to analytically depict a nonlinear Rayleigh wave, for assessing material nonlinearity. However, this analytical solution is applicable to a nonlinear Rayleigh wave scattered by damage which can be simplified as holistic material degradation at a sufficient degree, and may not be tenable when extened to evaluation of a single, localized micro-crack that is inadequate to perturb mechanical properties of the entire waveguide.

It is in recent that the authors of this paper have interrogated the second harmonic generation of Lamb waves (plate waves) induced by a fatigue crack with breathing behavior, by equating the fatigue crack as an additional wave source in addition to the original incident wave, and considering the crack-induced second harmonic as the radiation by the equivalent forces at the two crack surfaces [14]. A closed-form solution to the amplitude of the crack-induced second harmonic is obtained by virtue of the elastodynamic reciprocity theorem. Nonetheless, an explicit, analytical solution to the scattering problem of Rayleigh waves upon interaction with a surface or a sub-surface micro-crack and the solution to the crack-induced second harmonic generation is still beyond reach. To this end, the elastodynamic reciprocity theorem, along with a virtual wave approach, has been extended to Rayleigh waves in this study, to depict propagation of Rayleigh waves scattered by a 'breathing' crack, and the crack-induced nonlinearity in waves. The second harmonics generated by a surface crack and a sub-surface crack are modeled analytically, and the harmonic magnitudes are quantified, leading to a full analytical solution to nonlinear Rayleigh wavefield in the crack vicinity. Proof-of-concept numerical simulation is conducted to validate the analytical model and the solution.

This paper is structured as follows: in Section 2, the displacement and stress fields of a Rayleigh wave, under a 2D plane strain condition, are briefed, on which basis the new analytical solution is derived. The problem of the crack-induced second harmonic generation is stated in Section 3, followed with detailed solution to harmonic magnitude that is premised on the elastodynamic reciprocity theorem, decomposition principle and a virtual wave approach, in Section 4. Section 5 compares analytical and numerical results, to demonstrate the validity of the analytical model and the solution.

2. Analytical Depiction of Rayleigh Wavefield – Theoretical Foundation

Irrespective that considerable literature exists addressing propagation of the Rayleigh wave in an isotropic, homogenous, and linearly elastic solid [44], it is incumbent on us to recapitulate the fundamentals of Rayleigh waves, on which the model and solution to nonlinear interaction between a Rayleigh wave and a surface or sub-surface crack are to be developed.

In a 2D, half-space defined by $x-z$ coordinates, the displacements of a time-harmonic Rayleigh wave in an isotropic, homogenous, and linearly elastic waveguide can be defined, along the positive x direction, as

$$u_x(x,z) = \pm i A_{in} U^R(z) e^{\pm ikx}, \tag{1a}$$

$$u_z(x,z) = A_{in} W^R(z) e^{\pm ikx}. \tag{1b}$$

In the above, A_{in} signifies the magnitude of the incident Rayleigh wave, i the imaginary unit and ω the circular frequency. k is the wavenumber ($k=\omega / c_R$, where c_R denotes the phase velocity of Rayleigh wave). $u_x(x,z)$ and $u_z(x,z)$ represent the particulate displacement components of the Rayleigh wave in the x direction and z direction, respectively. The plus and minus signs in Eq. (1a) indicate wave propagation in the positive and negative x direction, respectively. Functions $U^R(z)$ and $W^R(z)$ read

$$U^R(z) = d_1 e^{-pz} + d_2 e^{-qz}, \tag{2a}$$

$$W^R(z) = d_3 e^{-pz} + e^{-qz}, \tag{2b}$$

where

$$d_1 = -(k^2+q^2)/(2kp), \tag{3a}$$

$$d_2 = q/k, \tag{3b}$$

$$d_3 = (k^2+q^2)/(2k^2). \tag{4}$$

p and q are given by

$$p^2 = k^2(1-c_R^2/c_L^2), \tag{5a}$$

$$q^2 = k^2(1-c_R^2/c_T^2), \tag{5b}$$

where $c_L = \sqrt{(\lambda+2\mu)/\rho}$ and $c_T = \sqrt{\mu/\rho}$ are the phase velocities of the longitudinal and transverse waves propagating along the positive x direction, respectively. λ and μ are Lame constants, and ρ the density of the waveguide.

Analogous to displacement components, the stress components of the Rayleigh wave can be obtained using the same approach, as

$$\tau_{xx} = A_{in} T_{xx}(z) e^{\pm ikx}, \tag{6a}$$

$$\tau_{xz} = \tau_{zx} = \pm i A_{in} T_{xz}(z) e^{\pm ikx}, \tag{6b}$$

$$\tau_{zz} = A_{in} T_{zz}(z) e^{\pm ikx}, \tag{6c}$$

where

$$T_{xx}(z) = \mu(d_4 e^{-pz} + d_5 e^{-qz}), \tag{7a}$$

$$T_{xz}(z) = \mu(d_6 e^{-pz} + d_7 e^{-qz}), \tag{7b}$$

$$T_{zz}(z) = \mu(d_8 e^{-pz} + d_9 e^{-qz}), \tag{7c}$$

and

$$d_4 = (k^2 + q^2)(2p^2 + k^2 - q^2)/(2pk^2), \tag{8a}$$

$$d_5 = \text{-}2q; \tag{8b}$$

$$d_6 = -d_7 = (k^2 + q^2)/k, \tag{9}$$

$$d_8 = -(k^2 + q^2)^2/(2pk^2), \tag{10a}$$

$$d_9 = 2q. \tag{10b}$$

Equations (1) and (6), respectively, depict the displacement and stress fields of an incident Rayleigh wave in an intact waveguide, serving as the theoretical foundation for the following derivation when a surface or sub-surface crack is present in the waveguide.

3. Crack-induced Second Harmonic of Rayleigh Wave

Consider a 2D, half-space waveguide, in which a surface crack at a microscopic degree (*e.g.*, an embryonic fatigue crack) exists, as illustrated schematically in **Fig. 1**. In practice, the crack surfaces are rough and the stress state in the vicinity of the crack under a cyclic load is complex.

The interaction of a probing Rayleigh wave with a surface/sub-surface crack and the according generation of nonlinear Rayleigh waves are the main focus of this study. Here, the crack surface, S_{crack}, is deemed smooth and in the absence of any external load. S_{crack} consists of two crack surfaces, namely S^{+}_{crack} and S^{-}_{crack}, respectively called the *positive surface* and *negative surface*. With the small dimension of the crack (crack depth is smaller than 1/5 of the wavelength of the incident Rayleigh wave) and ignorable gap between S^{+}_{crack} and S^{-}_{crack}, the crack opens and closes, respectively during the tensile and compressive phases of the Rayleigh wave. Owing to the displacement discontinuity at the crack location, the normal stress in the x direction on S^{+}_{crack}, as the Rayleigh wave traverses, shall satisfy the following 'traction-free' criterion:

$$\sigma_{xx}(z,t) \geq 0. \quad z \in S^{+}_{crack} \tag{11}$$

Thus, the compressive phase of the incident Rayleigh wave propagates through the crack without distortion, while the tensile phase is intercepted by the crack.

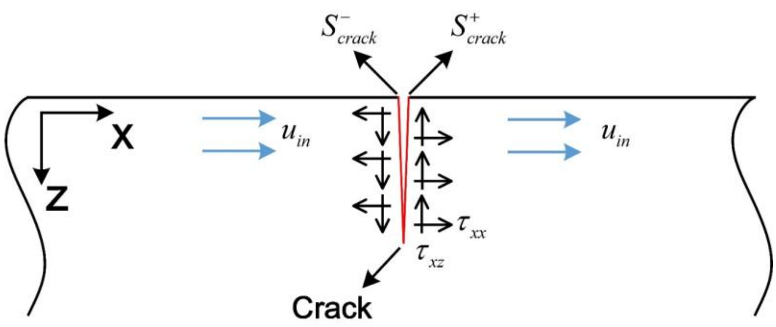

Figure 1. Schematic of propagation of incident Rayleigh wave in a 2D waveguide bearing a surface crack at a microscopic degree.

Allowing for the small dimension of the crack, a time-harmonic, concentrated force, $F(t)$, is introduced to reflect the perturbation of the crack to the original incident Rayleigh wavefield. Considering the microscopic dimensions of the crack, $F(t)$ is applied along x direction at the center of the crack. The magnitude of $F(t)$ equals to the difference in the integral value of the normal stresses in x direction on S_{crack}^{+} when the waveguide is in its intact status and bears a surface crack, respectively, as

$$
\begin{aligned}
F(t) &= \int_{S_{crack}^{+}} \sigma_{xx}(z,t)_{intact}\, ds - \int_{S_{crack}^{+}} \sigma_{xx}(z,t)_{cracked}\, ds \\
&= \begin{cases} 0, & \textit{during compressive phase} \\ \int_{S_{crack}^{+}} \sigma_{xx}(z,t)_{intact}\, ds. & \textit{during tensile phase} \end{cases}
\end{aligned}
\tag{12}
$$

In the above, $\sigma_{xx}(z,t)_{cracked}$ represents the normal stress component on S_{crack}^{+} in the waveguide bearing the crack, and $\sigma_{xx}(z,t)_{intact}$ signifies the normal stress component on the same surface in the intact waveguide. $F(t)$ serves as an additional wave source that is applied to the original incident Rayleigh wavefield, and thus $F(t)$ is referred to as the *second excitation force* in this study hereinafter. The second excitation force is present during the tensile phase in a cycle of wave propagation, and vanishes otherwise, as shown in **Fig. 2(a)**.

In the frequency domain, the second excitation force is decomposed into two equivalent forces: i) the first equivalent force, F_{eq1}, which is a sinusoidal signal at the excitation frequency ω of the incident Rayleigh wave; and ii) the second equivalent force, F_{eq2}, which is the absolute value of F_{eq1} at the double excitation frequency 2ω, as shown in **Figs. 2 (b-c)**. Either magnitude of F_{eq1} and F_{eq2} is half the magnitude of $F(t)$, whereby to warrant that the summation of F_{eq1} and F_{eq2} equates F. With this, F_{eq2} represents the source of the crack-induced second harmonic in the Rayleigh wavefield. Applied with the continuous-time Fourier transform (FT), it can be observed in **Fig. 2 (d)** that F_{eq1} corresponds to a wave component at the fundamental frequency (ω), and F_{eq2} to a wave component at 2ω – the source to generate the second harmonic.

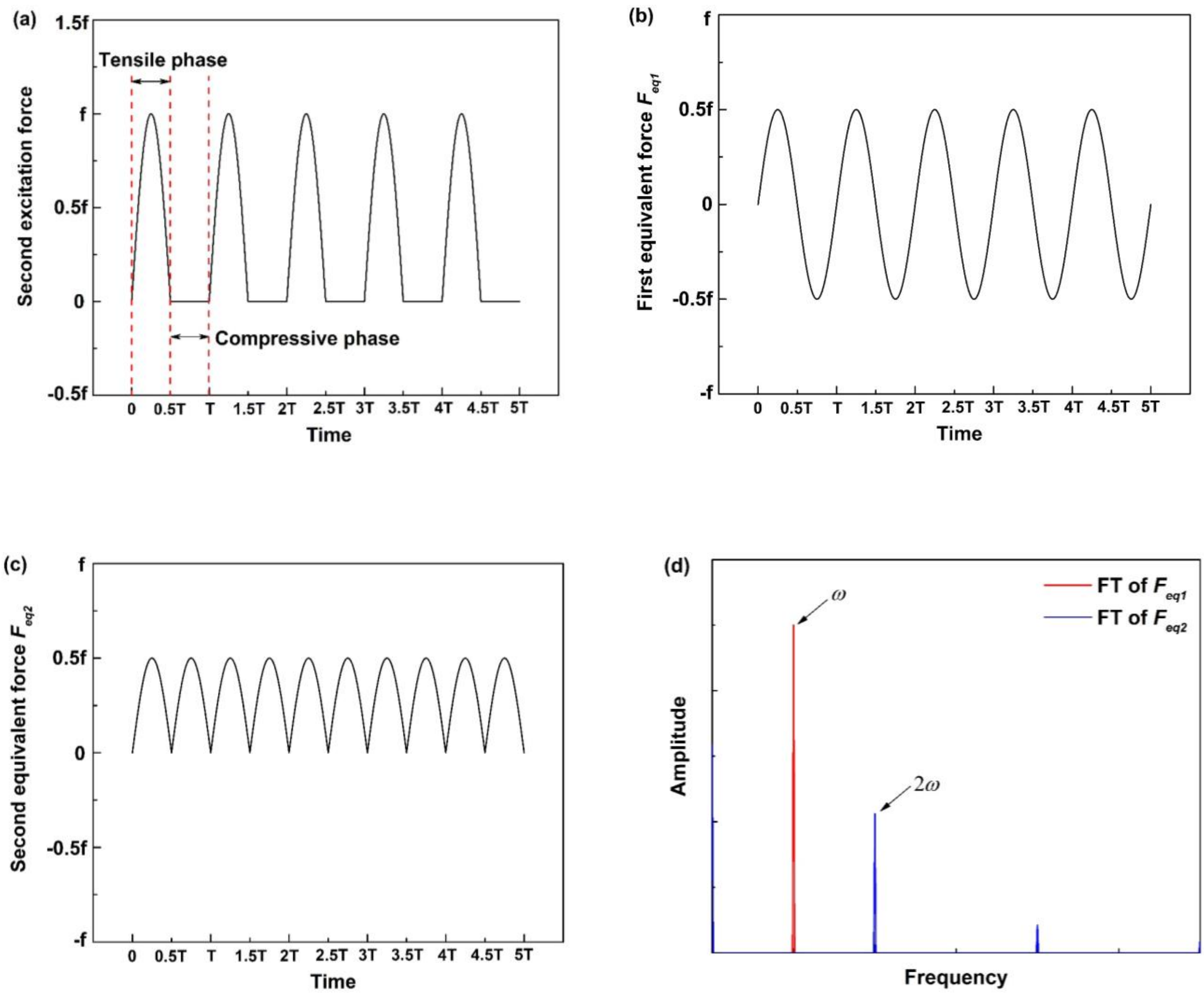

Figure 2. Time domain signals of (a) $F(t)$ applied on S^{+}_{crack}, (b) F_{eq1}, (c) F_{eq2}, and (d) spectra of F_{eq1} and F_{eq2} (ω: fundamental excitation frequency; 2ω: double excitation frequency).

To obtain the explicit solution to the crack-induced second harmonic of Rayleigh wave with the application of elastodynamic reciprocity theorem, the second excitation force is written in the form of stress tensor. Taking into account both the opening and closing phases of the crack during a cycle of the incident Rayleigh wave propagation, the stress components induced at S^{+}_{crack} and S^{-}_{crack} are written with an indicator function, as

$$\tau_{xx}^{breathing} = \tau_{xx} \cdot f(t), \tag{13a}$$

$$\tau_{xz}^{breathing} = \tau_{xz}^{breathing} = \tau_{xz} \cdot f(t), \tag{13b}$$

$$\tau_{zz}^{breathing} = \tau_{zz} \cdot f(t), \tag{13c}$$

where $\tau_{ij}\,(i,j=x,z)$ signifies the stress fields generated by the incident Rayleigh wave in the intact waveguide, $\tau_{ij}^{breathing}(i,j=x,z)$ represents the stress components at S_{crack}^{+} and S_{crack}^{-}, and the indicator function is

$$f(t)=\begin{cases}0, & crack\ opening\\ 1. & crack\ closing\end{cases} \tag{14}$$

Regulated by the indicator function as defined by Eq. (14), Eq. (13) – namely the incident Rayleigh wave-induced stress at S_{crack}^{+} and S_{crack}^{-}, can be decomposed into two equivalent stress fields, as

$$\tau_{xx}^{(1)}=\frac{1}{2}\tau_{xx}=\frac{1}{2}A_{in}T_{xx}(z)e^{i(kx-\omega t)}, \tag{15a}$$

$$\tau_{xz}^{(1)}=\tau_{zx}^{(1)}=\frac{1}{2}\tau_{xz}=\frac{i}{2}A_{in}T_{xz}(z)e^{i(kx-\omega t)}, \tag{15b}$$

$$\tau_{zz}^{(1)}=\frac{1}{2}\tau_{zz}=\frac{1}{2}A_{in}T_{zz}(z)e^{i(kx-\omega t)}, \tag{15c}$$

and

$$\tau_{xx}^{(2)}=\left|\tau_{xx}^{(1)}\right|, \tag{16a}$$

$$\tau_{xz}^{(2)}=\tau_{zx}^{(2)}=\left|\tau_{xz}^{(1)}\right|=\left|\tau_{zx}^{(1)}\right|, \tag{16b}$$

$$\tau_{zz}^{(2)}=\left|\tau_{zz}^{(1)}\right|. \tag{16c}$$

In the above, $\tau_{ij}^{(1)}(i,j=x,z)$ and $\tau_{ij}^{(2)}(i,j=x,z)$ signify the first and second equivalent stresses, respectively. The first equivalent stress, $\tau_{ij}^{(1)}$, induces the scattering wave at the excitation frequency ω, and the second equivalent stress, $\tau_{ij}^{(2)}$, generates the second harmonic wave at double excitation frequency 2ω, as illustrated schematically in **Fig. 3**.

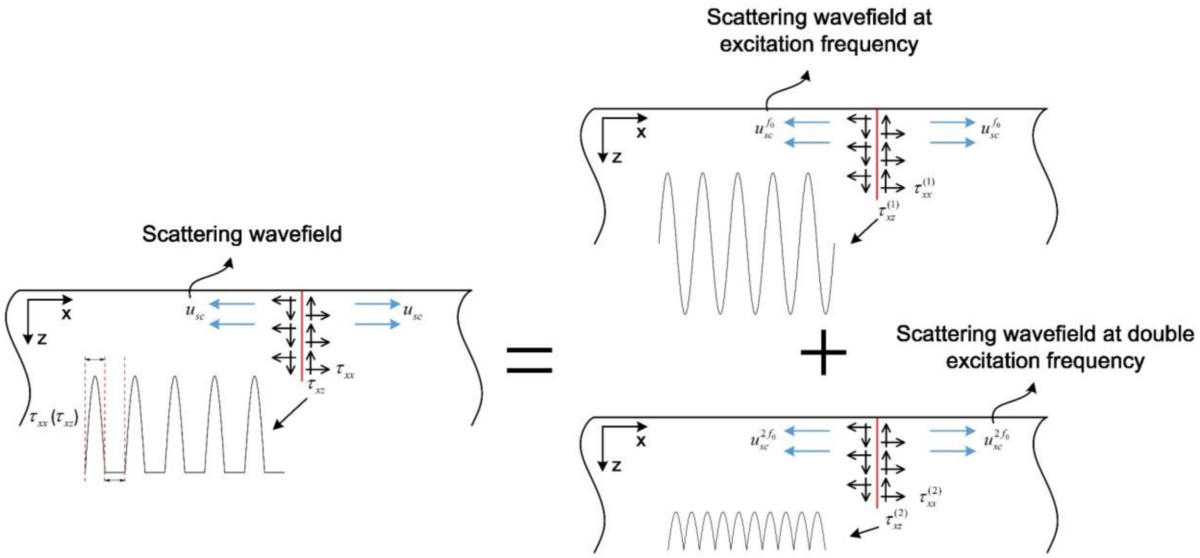

Figure 3. Principle of decomposition for the incident Rayleigh wave scattered by S^{+}_{crack} and S^{-}_{crack} of a 'breathing' crack ($u^{f_0}_{sc}$: scattering wavefield at excitation frequency ω, $u^{2f_0}_{sc}$: scattering wavefield at double excitation frequency 2ω).

4. Elastodynamic Reciprocity Theorem-based Solution

Subsequent to the above derivation, the elastodynamic reciprocity theorem, in conjunction with the use of a virtual wave method, is recalled, to determine the magnitude of the second harmonic induced by $\tau^{(2)}_{ij}$. The reciprocal identity relates two elastodynamic states of the body of an arbitrarily selected region in the waveguide. For the body of region V with the boundary P , under two distinct elastodynamic states denoted by A and B , it has

$$\int_V (f_i^A u_i^B - f_i^B u_i^A) dV = \int_P (u_i^A \sigma_{ij}^B - u_i^B \sigma_{ij}^A) n_j dP, \tag{17}$$

where f_i^A and f_i^B are the body forces, u_i^A and u_i^B the displacements, σ_{ij}^A and σ_{ij}^B the stress and n_j the components of the outward normal to P , respectively, under states *A* and *B*. In this study, state A is the crack-scattered second harmonic of the Rayleigh wave that is generated by $\tau^{(2)}_{ij}$, and state B is a virtual Rayleigh wave, which propagates in the negative x direction.

Based on the Rayleigh wavefields descripted in Section 2, the displacement and stress fields of the Rayleigh wave, under states A and B, can be obtained. For the forward-propagating, crack-induced second harmonic, it has

$$u_x^{2\omega+} = iA_{2\omega} U^R(z) e^{ikx}, \tag{18a}$$

$$u_z^{2\omega+} = A_{2\omega} W^R(z) e^{ikx}; \tag{18b}$$

$$\tau_{xx}^{2\omega+} = A_{2\omega} T_{xx}(z) e^{ikx}, \tag{19a}$$

$$\tau_{xz}^{2\omega+} = iA_{2\omega} T_{xz}(z) e^{ikx}; \tag{19b}$$

for the back-propagating, crack-induced second harmonic, one has

$$u_x^{2\omega-} = -iA_{2\omega} U^R(z) e^{-ikx}, \tag{20a}$$

$$u_z^{2\omega-} = A_{2\omega} W^R(z) e^{-ikx}; \tag{20b}$$

$$\tau_{xx}^{2\omega-} = A_{2\omega} T_{xx}(z) e^{-ikx}, \tag{21a}$$

$$\tau_{xz}^{2\omega-} = -iA_{2\omega} T_{xz}(z) e^{-ikx}. \tag{21b}$$

In the above, $u_i^{2\omega+} (u_i^{2\omega-})$ and $\tau_{ij}^{2\omega+} (\tau_{ij}^{2\omega-})$ represent the displacement and stress fields of the second harmonic, respectively, and the plus (or minus) sign implies that the second harmonic propagates in the positive (or negative) direction. $A_{2\omega}$ is the magnitude coefficient of the crack-scattered second harmonic wave.

In the elastodynamic reciprocity theorem-based modeling, for the virtual wave (*i.e.*, state B), the displacement and stress fields can be expressed as

$$u_x^{vi} = -iB^{vi} U^R(z) e^{-ikx}, \tag{22a}$$

$$u_z^{vi} = B^{vi} W^R(z) e^{-ikx}; \tag{22b}$$

$$\tau_{xx}^{vi} = B^{vi} T_{xx}(z) e^{-ikx}, \tag{23a}$$

$$\tau_{xz}^{vi} = -iB^{vi} T_{xz}(z) e^{-ikx}, \tag{23b}$$

where B^{vi} is the magnitude coefficient of the virtual wave. By introducing the virtual wave into Eq. (17), the magnitude of the crack-induced second harmonic can be ascertained explicitly (note: the unknown magnitude coefficient of the virtual wave, B^{vi}, is to be canceled in the subsequent derivation).

Consider the crack vicinity – the region V with the boundary P (edge 1~7) encompassing the crack, as shown in **Fig.4**. Provided the thickness of V is sufficiently large (*e.g.*, greater than three times the wavelength of the incident Rayleigh wave), the Rayleigh wave attenuates to vanish at the bottom of the region (*i.e.*, edge 2). Here, the contour integration in the right-hand side of Eq. (17) at edge i is denoted as J_i ($i = 1, 2, ..., 7$). As there is no body force existing in both states (*A* and *B*), the left-hand side of Eq. (17) equals zero. Due to the exponential decay of the Rayleigh wave in the waveguide thickness direction, J_2 retreats to zero. On the other hand, as the top surface of the waveguide is traction-free, one has that $J_4 = J_7 = 0$. As demonstrated elsewhere [45], the contour integral in the right-hand side of Eq. (17) is non-zero only when propagation directions of two waves used in the elastodynamic reciprocity theorem are opposite simultaneously. As a consequence, there is no contribution from edge 1 to the integral in the right-hand side of Eq. (17) (*i.e.*, $J_1 = 0$), because the propagation directions of both the virtual wave and crack-scattered second harmonic are in the negative x direction along edge 1. With this, Eq. (17) yields to

$$J_3 + J_5 + J_6 = 0, \tag{24}$$

where

$$\begin{aligned} J_3 &= \int_0^\infty (u_x^{2\omega+}\tau_{xx}^{vi} + u_z^{2\omega+}\tau_{xz}^{vi} - u_x^{vi}\tau_{xx}^{2\omega+} - u_z^{vi}\tau_{xz}^{2\omega+}) \cdot (+1) \cdot dz \\ &= 2iA_{2\omega}B^{vi}I, \end{aligned} \tag{25}$$

and

$$I = \int_0^\infty [W^R(z)T_{xz}(z) - U^R(z)T_{xx}(z)] \cdot dz. \tag{26}$$

For J_5 and J_6, it has

$$J_5 = \int_0^L \xi^+ \cdot (-1) \cdot dz, \tag{27}$$

$$J_6 = \int_0^L \xi^- \cdot (+1) \cdot dz, \tag{28}$$

where L is the crack length – the crack severity along the waveguide thickness, and

$$\xi^+ = u_x^{2\omega+}\tau_{xx}^{vi} + u_z^{2\omega+}\tau_{xz}^{vi} - u_x^{vi}\tau_{xx}^{2\omega+} + u_z^{vi}\tau_{xz}^{2\omega+}, \tag{29a}$$

$$\xi^- = u_x^{2\omega-}\tau_{xx}^{vi} + u_z^{2\omega-}\tau_{xz}^{vi} - u_x^{vi}\tau_{xx}^{2\omega-} + u_z^{vi}\tau_{xz}^{2\omega-}. \tag{29b}$$

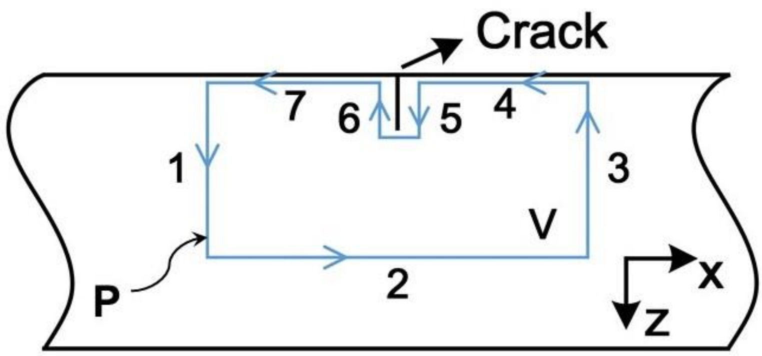

Figure 4. Integral domain of the crack vicinity.

Focusing on the normal traction at the two crack surfaces first, one has that $\tau_{xz}^{2\omega+} = \tau_{xz}^{2\omega-} = 0$, $u_z^{2\omega+} = u_z^{2\omega-}$ and $\tau_{xx}^{2\omega+} = \tau_{xx}^{2\omega-}$, due to the symmetric motion of particles at the two crack surfaces with respect to z axis. Thus, Eq. (24) can be written as

$$2iA_{2\omega}B^{vi}I - B^{vi}\int_0^L \Delta u_x^{2\omega} T_{xx}(z)dz = 0, \tag{30}$$

where $\Delta u_x^{2\omega}$ is the crack opening displacement in x direction, as

$$\Delta u_x^{2\omega} = u_x^{2\omega+} - u_x^{2\omega-}. \tag{31}$$

The magnitude coefficient, $A_{2\omega}$, is determined as

$$A_{2\omega} = \frac{1}{2iI}\int_0^L \Delta u_x^{2\omega} T_{xx}(z)dz. \tag{32}$$

For a surface crack of small dimensions, the opening displacement of the crack, from the normal stress component $\tau_{xx}^{(2)}$, can be expressed as [46]

$$\Delta u_x(z) = \frac{4L}{E'}\tau_{xx}^{(2)}\sqrt{1-(\frac{z}{L})^2}, \tag{33}$$

where

$$E' = \begin{cases} E, & \textit{for plane stress} \\ \dfrac{E}{(1-\nu^2)}. & \textit{for plane strain} \end{cases} \tag{34}$$

Substituting Eqs. (16) and (33) into Eq. (32) yields

$$A_{2\omega} = \frac{\pi(1-\nu)L^2 A_{in}[T_{xx}(L/2)]^2}{8i\mu I}. \tag{35}$$

An analogous solution to the shear stress component, $\tau_{xz}^{(2)}$, can also be obtained as

$$A_{2\omega} = \frac{\pi(1-\nu)L^2 A_{in}[T_{xz}(L/2)]^2}{8i\mu I}. \tag{36}$$

Combining Eqs. (35) and (36), the magnitude of the displacement of the second harmonic generated by a surface crack can be determined, in an explicit manner, as

$$u_x^{2\omega} = \frac{\pi(1-\nu)L^2 A_{in}\{[T_{xx}(L/2)]^2 - [T_{xz}(L/2)]^2\}}{8\mu I} U^R(z)e^{ikx}, \tag{37}$$

$$u_z^{2\omega} = \frac{i\pi(1-\nu)L^2 A_{in}\{[T_{xx}(L/2)]^2 - [T_{xz}(L/2)]^2\}}{8\mu I} W^R(z)e^{ikx}. \tag{38}$$

Equations (37) and (38), explicitly and analytically, link the length of a surface crack (*i.e.*, L), to the crack-scattered second harmonic wavefield, on which basis the crack can be evaluated inversely.

Along the same line of thinking, expanding the above discussion from a surface crack to an interior sub-surface crack that is beneath the waveguide surface, the crack opening displacements due to the normal and shear components can be written as

$$\Delta u_x(z) = \frac{2L}{E'}\tau_{xx}^{(2)}\sqrt{1-(\frac{z-d}{L/2})^2}, \tag{39}$$

$$\Delta u_z(z)=\frac{2L}{E'}\tau_{xz}^{(2)}\sqrt{1-(\frac{z-d}{L/2})^2}, \tag{40}$$

where d defines the location of the crack along the waveguide thickness, as illustrated schematically in **Fig. 5**.

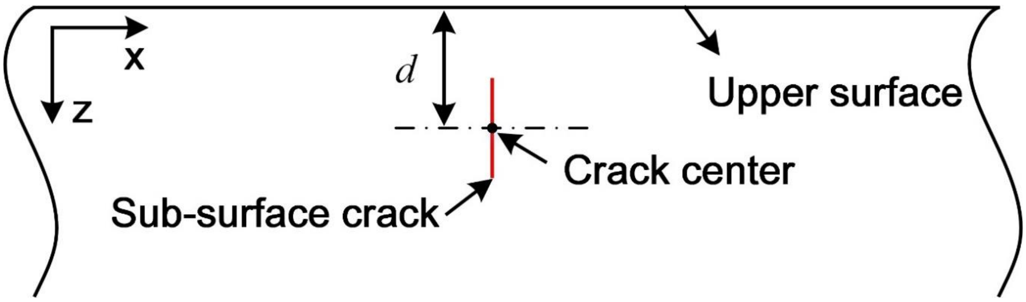

Figure 5. Schematic of a sub-surface crack in the waveguide.

Substituting Eqs. (39) and (40) into Eq. (32) leads to the displacement magnitudes of the second harmonic generated by the sub-surface crack, as

$$u_x^{2\omega}=\frac{\pi(1-\nu)L^2A_{in}\{[T_{xx}(d)]^2-[T_{xz}(d)]^2\}}{16\mu I}U^R(z)e^{ikx}, \tag{41}$$

$$u_z^{2\omega}=\frac{i\pi(1-\nu)L^2A_{in}\{[T_{xx}(d)]^2-[T_{xz}(d)]^2\}}{8\mu I}W^R(z)e^{ikx}. \tag{42}$$

In the same vein, Eqs (41) and (42) correlate the second harmonic wavefield induced by a sub-surface crack with the crack length, in an explicitly and analytically manner, which are therefore conducive to the evaluation of crack length, even when the crack is a sub-surface crack that is invisible. It is noteworthy that in the above analytical modeling, the second harmonic generation of Rayleigh waves are induced by the 'breathing' and rubbing motions of surface/sub-surface cracks. Contribution of nonlinear elasticity of the waveguide to the nonlinear Rayleigh generation is neglected due to its neglectable effect compared with that of crack-induced nonlinearity.

5. Proof-of-Concept Validation Using Numerical Simulation

Finite element (FE) simulation is performed with ABAQUS®/EXPLICIT to validate the analytical solutions: Eqs. (37) and (38) for a surface crack, and Eqs. (41) and (42) for an interior sub-surface crack.

A 2D waveguide, identical to that used in the theoretical derivation, is considered, and the FE model is developed. With aluminum (density: 2700 kg/m3; Young's modulus: 73 GPa; Poisson's ratio: 0.33) as the waveguide material, velocities of the longitudinal and transverse waves are 6,329 m/s and 3,188 m/s, respectively. The incident Rayleigh wave is excited by applying a displacement field with the magnitude of 1×10^{-4} mm at a FE node on the upper surface of the FE model, and Rayleigh wave propagation is captured 100 mm from the excitation.

According to the phase velocity of a Rayleigh wave [30]

$$(2-c_R^2/c_T^2)^2-4(1-c_R^2/c_L^2)^{1/2}(1-c_R^2/c_T^2)^{1/2}=0, \tag{43}$$

the phase velocity of the incident Rayleigh wave is calculated to be 2,971 m/s. Three different excitation frequencies are considered, namely 500 kHz, 800 kHz and 1 MHz (with corresponding wavelengths being 5.942 mm, 3.714 mm and 2.971 mm, respectively). To warranty simulation accuracy, the integral step is 0.2 ns and a fine FE mesh is applied in which the maximum mesh size is 0.1 mm – that is ~1/30 of the minimal wavelength of the Rayleigh wave. By setting an absorbing layer with increasing damping (ALID) [47] on the bottom of the FE model, the wave reflection from the lower surface is eliminated. To simulate the 'breathing' behavior of the crack that introduces nonlinearity to the incident Rayleigh wave, the contact-pair interaction-based boundary condition is applied on the two crack surfaces, with which the separation of the two crack surfaces is permitted, while penetration of FE nodes on the two surfaces is prevented.

First, the second harmonic of Rayleigh wave generated by a surface crack is scrutinized. The crack length varies from 0.1 to 0.6 mm, with an interval of 0.1 mm. The analytical and numerical results of magnitude of the crack-induced second harmonic are compared in **Fig. 6**, for three selected frequencies.

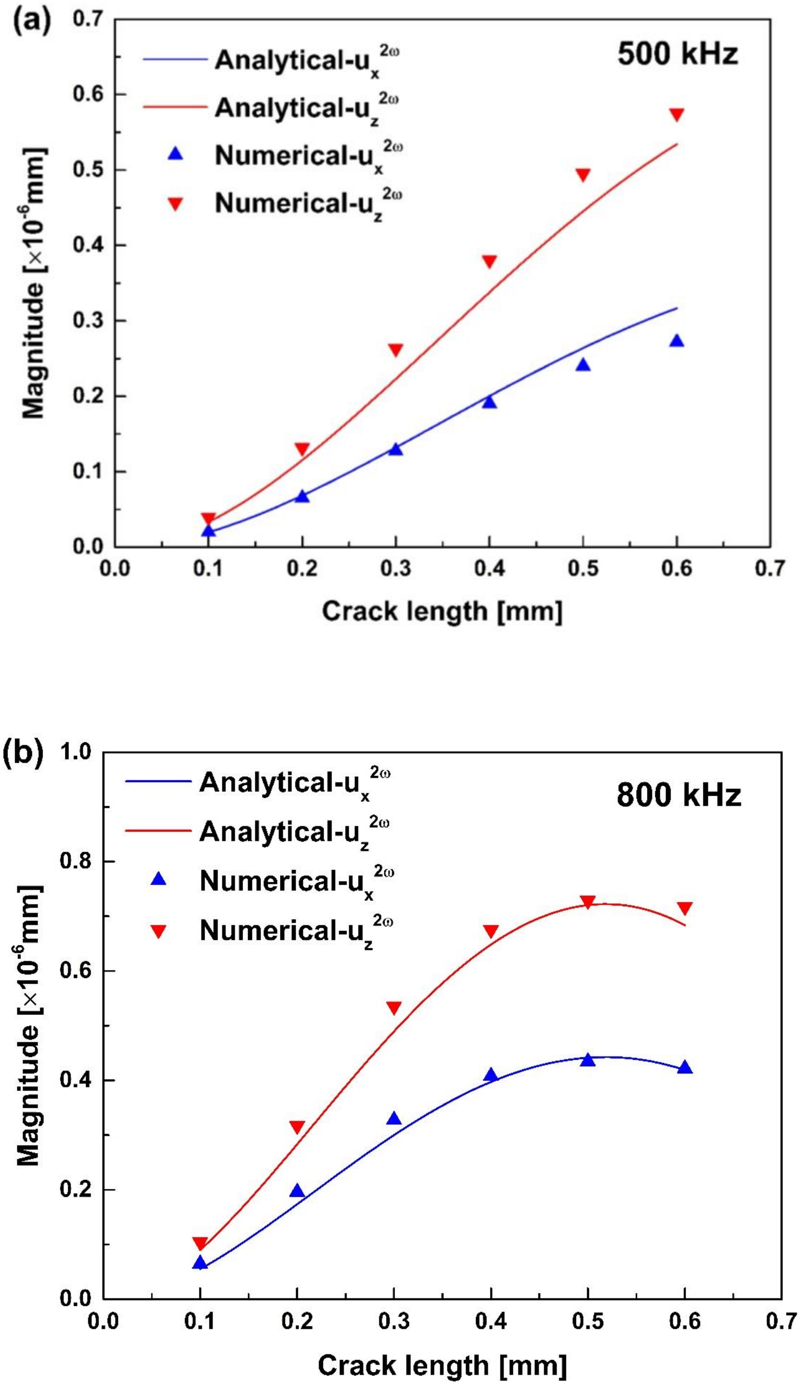

Figure 6. Comparison of analytical and numerical results when the frequency of incident Rayleigh surface wave is (a) 500 kHz, (b) 800 kHz, and (c) 1 MHz.

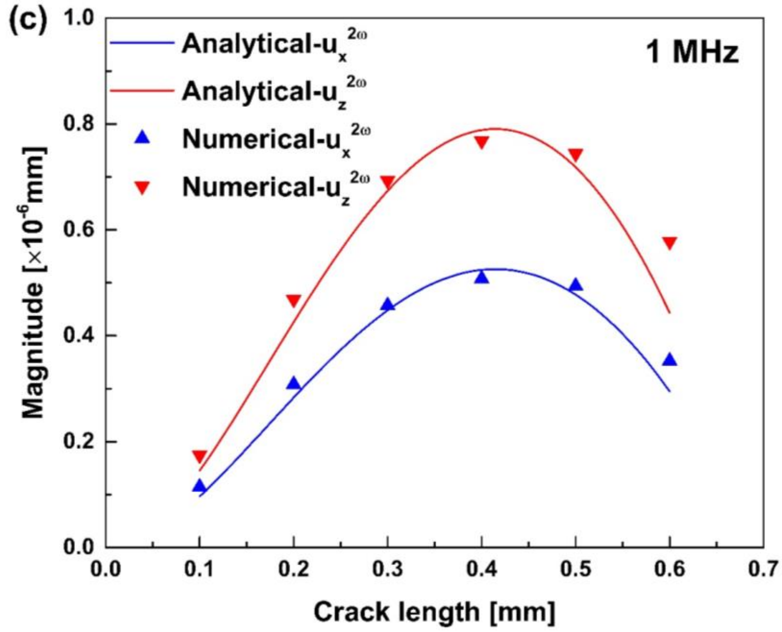

Figure 6. *Cont.*

Figure 6 reveals that variations in magnitude of the second harmonic induced by a surface crack, as the crack progresses, are distinct at different frequencies. At 500 kHz, the magnitude increases monotonously against the crack length in both x and z directions, in **Fig. 6(a)**, while the magnitude, at 800 kHz and 1 MHz, increases against the crack length, reaches its maximum and then decreases, **Figs. 6(b-c)**. The non-monotonous variation at higher frequencies can be attributed to the distinct stress distributions along the waveguide thickness at different excitation frequencies. Putting into perspective, the normal and shear stress components along the waveguide thickness at the three frequencies, analytically calculated based on Eqs. (6a) and (6b), are illustrated in **Fig. 7**. It can be observed that at 500 kHz the normal and shear stress components slightly decrease and increase, respectively, with respect to the crack depth, making magnitude of the second harmonic largely depend on the crack length, according to Eqs. (37) and (38), and thus the magnitude monotonously increases against the crack length. On the other hand, the normal and shear stress components dramatically decrease and increase in the sub-surface region at 800 kHz and 1 MHz, leading to non-monotonic variation between magnitude of the second harmonic and the crack length. **Figure 8** presents numerical results of stress distributions of the incident Rayleigh wave, demonstrating the above interpretation.

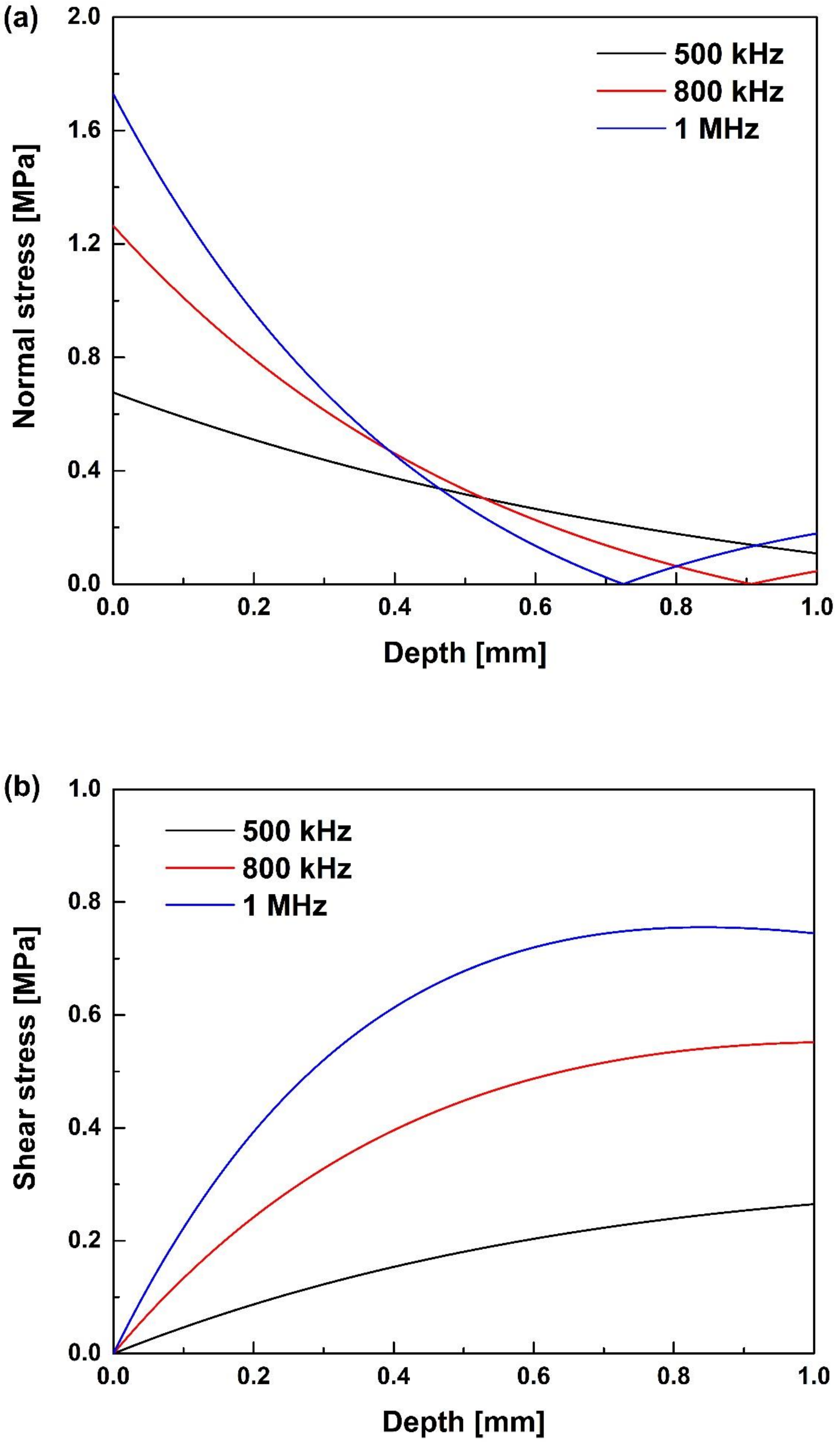

Figure 7. Analytically obtained (a) normal and (b) shear stress distributions along waveguide thickness when the frequency of incident Rayleigh surface wave is 500 kHz, 800 kHz, and 1 MHz.

Irrespective of the discrepancy in variation of the magnitude at different excitation frequencies, it can be observed that in both the x direction and z directions, numerical results agree well with the analytical results, precisely reflecting the variation of the second harmonic of a Rayleigh wave and validating the developed analytical solution to the magnitude of the second harmonic generated by a 'breathing' crack.

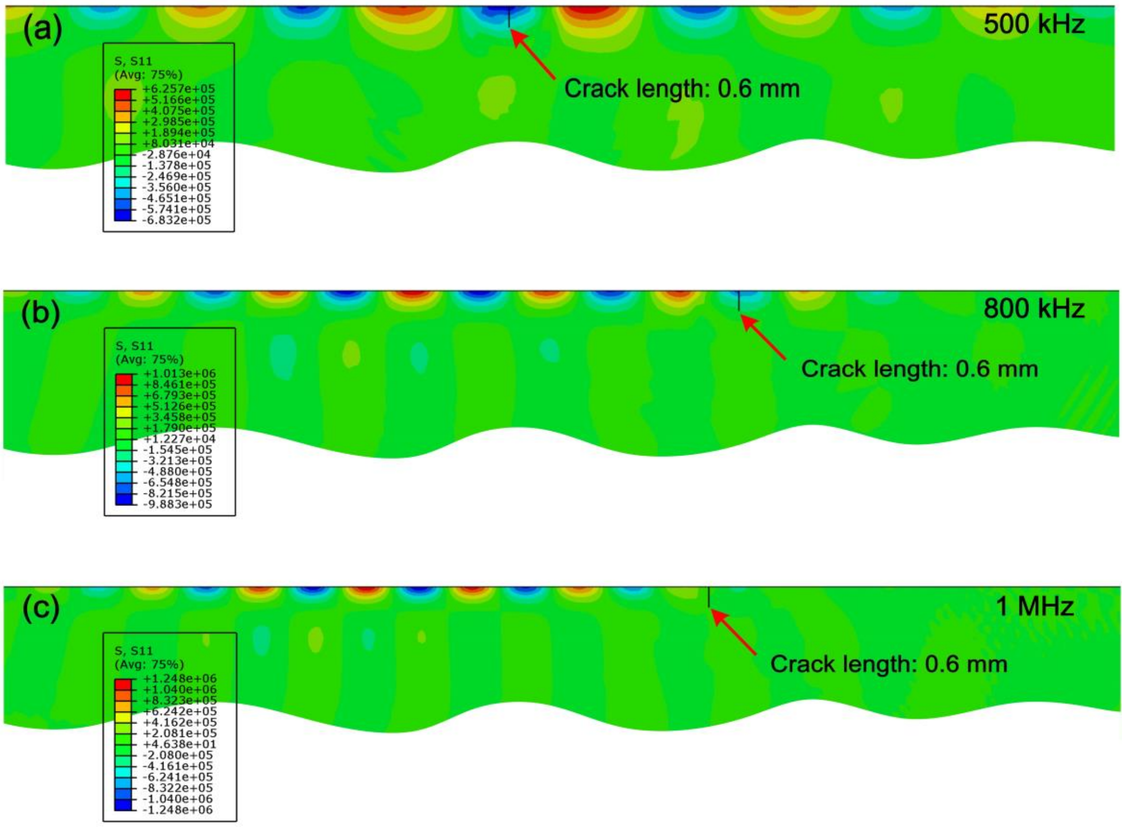

Figure 8. Numerically obtained normal stress distribution along waveguide thickness when the frequency of incident Rayleigh surface wave is (a) 500 kHz, (b) 800 kHz, and (c) 1 MHz.

To take a step further, the second harmonic generated by an interior sub-surface crack is investigated when the incident Rayleigh wave is excited at 500 kHz, as a representative. The crack center is respectively 0.3 mm, 0.6 mm and 1.0 mm deep to the upper surface of the waveguide, and the crack length varies from 0.1 mm to 0.5 mm with an increment of 0.1 mm. The analytical results obtained using Eqs. (41) and (42) and numerical results using the FE model are compared in **Fig. 9**. As can be seen, the magnitude of sub-surface crack-induced second harmonic increases monotonously against the crack length for sub-surface cracks at different depths in the waveguide thickness. The analytical and numerical results are in good agreement, demonstrating the theoretical modeling and solution (Eqs. (41) and (42)) are accurate to depict the nonlinear interaction between a Rayleigh wave and an interior sub-surface crack. It is noted in **Fig. 9** that at a given crack length, the magnitude of the second harmonic is smaller when the crack is deeper in the waveguide – a phenomenon that can be analytically interpreted in terms of the distribution of the normal stress and shear stress along the waveguide thickness, as obtained using Eqs. (6a) and (6b), and depicted in **Fig. 7**: the smaller difference between the normal and shear stress components at a deeper location leads to a smaller value of the term in the curly bracket in Eqs. (41) and (42).

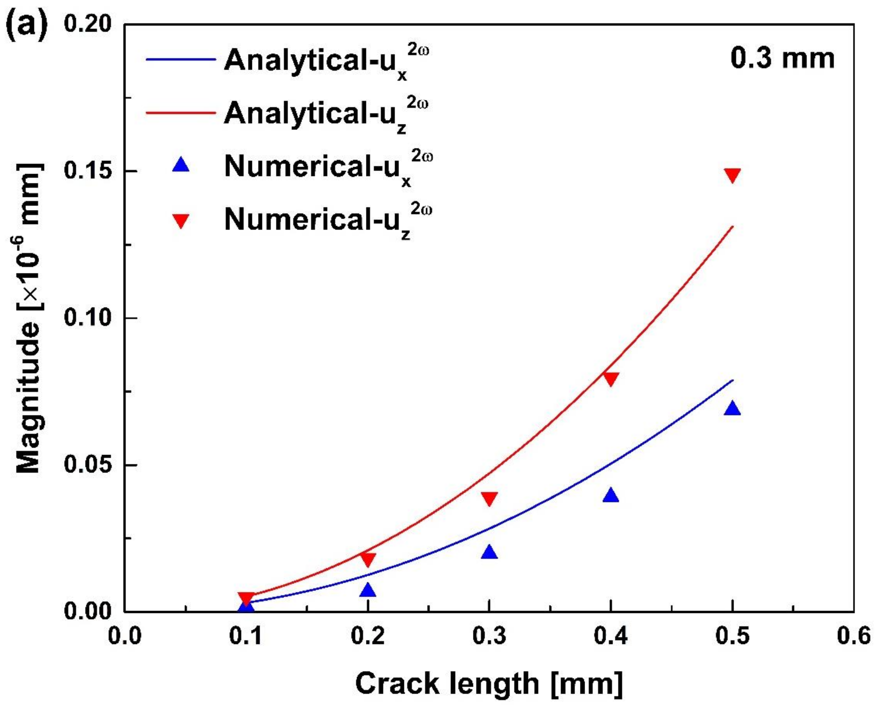

Figure 9. Comparison between analytical and numerical results when crack center is (a) 0.3 mm, (b) 0.6 mm, and (c) 1.0 mm from the upper surface of the waveguide.

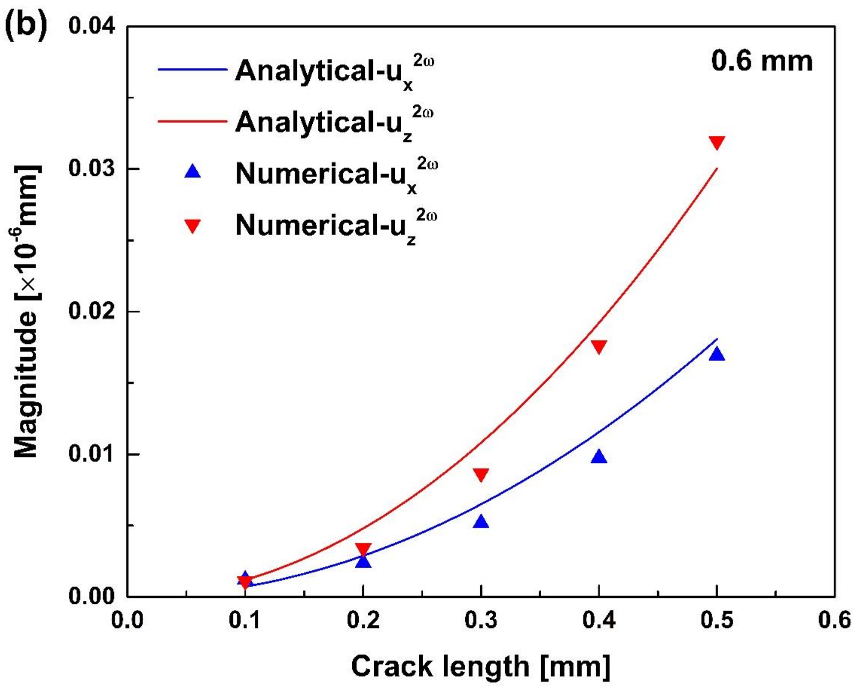

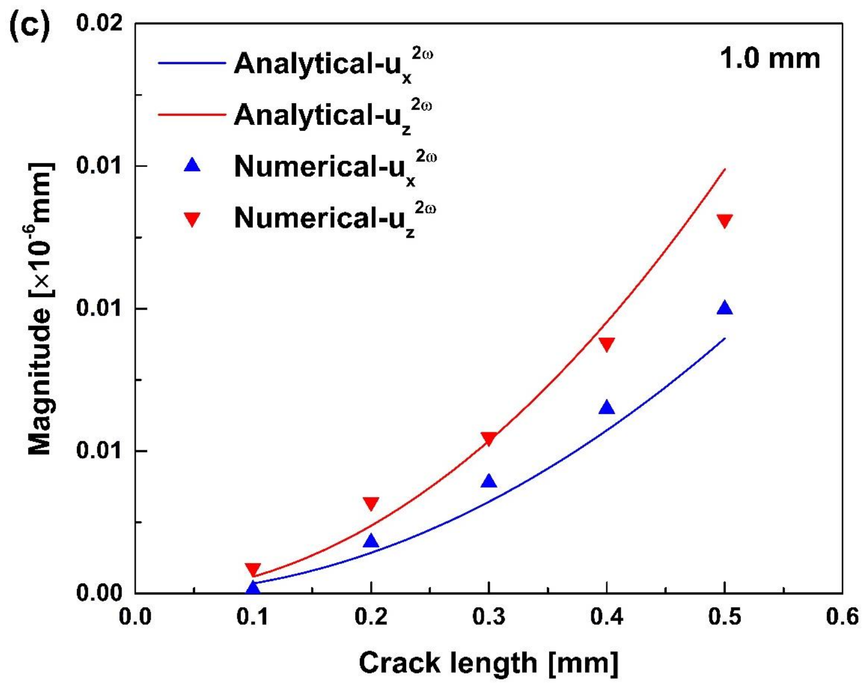

Figure 9. *Cont.*

The quantitative accordance between the analytical and numerical results has argued that the analytical model and solution derived in this study are able to explicitly quantify the magnitude of second harmonic of a Rayleigh wave induced by a surface or a sub-surface crack. The analytical modeling and explicit solution to the second harmonic generation of Rayleigh waves can facilitate detection of cracks in early stage and offer theoretical foundation and guidance to the implementation of damage characterization framework based on nonlinear Rayleigh waves.

6. Concluding Remarks

Rayleigh wave scattered by a surface or a sub-surface micro-crack is investigated, based on the elastodynamic reciprocity theorem, in conjunction with a virtual wave approach. With it, the second harmonic triggered by the clapping and rubbing behavior of the micro-crack is quantified. The stress generated by the incident Rayleigh wave at the crack surface is decomposed into two equivalent stresses components and the second equivalent stress component is demonstrated as the source to induce second harmonics. Explicit expression for the magnitude of the second harmonic generated by a surface crack or a sub-surface crack is derived by applying the second equivalent stress into the elastodynamic reciprocity equation. Proof-of-concept numerical simulation is conducted to validate the analytical model and solution, and quantitative agreement between analytical and numerical results accentuates the validity and accuracy of the proposed method. From the perspective of fracture mechanics, a fatigue crack usually initiates 45 degree to the surface from slip-bands, and a sub-surface crack is normally located in the plane parallel to the waveguide surface. With appropriate coordinate transformation, analytical solutions obtained for vertical surface/sub-surface cracks in this study can be conveniently extended to inclined cracks and parallel cracks. The developed analytical model and solution are beneficial to early awareness and quantitative evaluation of embryonic cracks that are on or near to a structural surface.

Acknowledgement

The work was supported by a Key Project (No. 51635008) and General Project (No. 51875492) received from the National Natural Science Foundation of China. Z Su acknowledges the support from the Hong Kong Research Grants Council via General Research Funds (Nos. 15202820, 15204419 and 15212417).

References

[1] W. Li, Z. Lan, N. Hu, M. Deng, Modeling and simulation of backward combined harmonic generation induced by one-way mixing of longitudinal ultrasonic guided waves in a circular pipe, Ultrasonics 113 (2021) 106356.

[2] X. Yang, K. Wang, Y. Xu, L. Xu, W. Hu, H. Wang, Z. Su, A reverse time migration-based multistep angular spectrum approach for ultrasonic imaging of specimens with irregular surfaces, Ultrasonics 108 (2020) 106233.

[3] X. Yu, P. Zuo, J. Xiao, Z. Fan, Detection of damage in welded joints using high order feature guided ultrasonic waves, Mech. Syst. Sig. Process. 126 (2019) 176-192.

[4] Y.F. Lee, Y. Lu, R. Guan, Nonlinear guided waves for fatigue crack evaluation in steel joints with digital image correlation validation, Smart Mater. Struct. 29 (2020) 035031.

[5] Y. Ren, L. Qiu, S. Yuan, Z. Su, A diagnostic imaging approach for online characterization of multi-impact in aircraft composite structures based on a scanning spatial-wavenumber filter of guided wave, Mech. Syst. Sig. Process. 90 (2017) 44-63.

[6] Y. Shao, L. Zeng, J. Lin, W. Wu, H. Zhang, Trailing pulses self-focusing for ultrasonic-based damage detection in thick plates, Mech. Syst. Sig. Process. 119 (2019) 420-431.

[7] G. Tang, M. Liu, L.J. Jacobs, J. Qu, Detecting localized plastic strain by a scanning collinear wave mixing method, J. Nondestr. Eval. 33 (2014) 196-204.

[8] X. Sun, H. Liu, Y. Zhao, J. Qu, M. Deng, N. Hu, The zero-frequency component of bulk waves in solids with randomly distributed micro-cracks, Ultrasonics 107 (2020) 106172.

[9] H. Xu, L. Cheng, Z. Su, J.-L. Guyader, Identification of structural damage based on locally perturbed dynamic equilibrium with an application to beam component, J. Sound Vib. 330 (2011) 5963-5981.

[10] H. Cho, M. Hasanian, S. Shan, C.J. Lissenden, Nonlinear guided wave technique for localized damage detection in plates with surface-bonded sensors to receive Lamb waves generated by shear-horizontal wave mixing, NDT & E Int. 102 (2019) 35-46.

[11] C.A. Chua, P. Cawley, Crack growth monitoring using fundamental shear horizontal guided waves, Struct. Health Monitor. 19 (2020) 1311-1322.

[12] F. Zhu, E. Pan, Z. Qian, Y. Wang, Dispersion curves, mode shapes, stresses and energies of SH and Lamb waves in layered elastic nanoplates with surface/interface effect, Int. J. Eng. Sci. 142 (2019) 170-184.

[13] K. Wang, M. Liu, Z. Su, S. Yuan, Z. Fan, Analytical insight into “breathing” crack-induced acoustic nonlinearity with an application to quantitative evaluation of contact cracks, Ultrasonics 88 (2018) 157-167.

[14] L. Xu, K. Wang, X. Yang, Y. Su, J. Yang, Y. Liao, P. Zhou, Z. Su, Model-driven Fatigue Crack Characterization and Growth Prediction: A Two-step, 3-D Fatigue Damage Modeling Framework for Structural Health Monitoring, Int. J. Mech. Sci. (2020) 106226.

[15] L. Xu, Y. Su, K. Wang, X. Yang, S. Yuan, Z. Su, An Elastodynamic Reciprocity Theorem-based Closed-form Solution to Second Harmonic Generation of Lamb Waves by A Fatigue Crack: Theory & Experimental Validation, J. Sound Vib. (2021) 116226.

[16] H.J. Lim, H. Sohn, Online fatigue crack prognosis using nonlinear ultrasonic modulation, Struct. Health Monitor. 18 (2019) 1889-1902.

[17] H.J. Lim, H. Sohn, Y. Kim, Data-driven fatigue crack quantification and prognosis using nonlinear ultrasonic modulation, Mech. Syst. Sig. Process. 109 (2018) 185-195.

[18] Z. Su, L. Ye, Identification of damage using Lamb waves: from fundamentals to applications, Springer Science & Business Media, 2009.

[19] M.V. Wilde, M.V. Golub, A.A. Eremin, Experimental and theoretical investigation of transient edge waves excited by a piezoelectric transducer bonded to the edge of a thick elastic plate, J. Sound Vib. 441 (2019) 26-49.

[20] J.M. Hughes, M. Mohabuth, A. Kotousov, C.-T. Ng, The fundamental ultrasonic edge wave mode: Propagation characteristics and potential for distant damage detection, Ultrasonics 114 (2021) 106369.

[21] J.M. Hughes, M. Mohabuth, A. Khanna, J. Vidler, A. Kotousov, C.-T. Ng, Damage detection with the fundamental mode of edge waves, Struct. Health Monitor. 20 (2021) 74-83.

[22] M.V. Wilde, M.V. Golub, A.A. Eremin, Experimental observation of theoretically predicted spectrum of edge waves in a thick elastic plate with facets, Ultrasonics 98 (2019) 88-93.

[23] L. Yu, C.A. Leckey, Lamb wave–based quantitative crack detection using a focusing array algorithm, J. Intell. Mater. Syst. Struct. 24 (2013) 1138-1152.

[24] N. Toyama, J. Noda, T. Okabe, Quantitative damage detection in cross-ply laminates using Lamb wave method, Compos. Sci. Technol. 63 (2003) 1473-1479.

[25] K. Wang, Z. Fan, Z. Su, Orienting fatigue cracks using contact acoustic nonlinearity in scattered plate waves, Smart Mater. Struct. 27 (2018) 09LT01.

[26] J. Yang, J. He, X. Guan, D. Wang, H. Chen, W. Zhang, Y. Liu, A probabilistic crack size quantification method using in-situ Lamb wave test and Bayesian updating, Mech. Syst. Sig. Process. 78 (2016) 118-133.

[27] S. Yuan, J. Chen, W. Yang, L. Qiu, On-line crack prognosis in attachment lug using Lamb wave-deterministic resampling particle filter-based method, Smart Mater. Struct. 26 (2017) 085016.

[28] W. Cao, K. Wang, P. Zhou, X. Yang, L. Xu, M. Liu, P. Fromme, B. Pang, R. Chi, Z. Su, Nonlinear ultrasonic evaluation of disorderedly clustered pitting damage using an in situ sensor network, Struct. Health Monitor. 19 (2020) 1989-2006.

[29] K. Wang, W. Cao, L. Xu, X. Yang, Z. Su, X. Zhang, L. Chen, Diffuse ultrasonic wave-based structural health monitoring for railway turnouts, Ultrasonics 101 (2020) 106031.

[30] C. Wang, O. Balogun, J.D. Achenbach, Scattering of a Rayleigh wave by a near surface crack which is normal to the free surface, Int. J. Eng. Sci. 145 (2019) 103162.

[31] C. Yang, J.D. Achenbach, Time domain scattering of elastic waves by a cavity, represented by radiation from equivalent body forces, Int. J. Eng. Sci. 115 (2017) 43-50.

[32] O. Balogun, J.D. Achenbach, Application of the reciprocity theorem to scattering of surface waves by an inclined subsurface crack, Int. J. Solids Struct. 207 (2020) 82-88.

[33] T. Maruyama, Harmonic balance-boundary element and continuation methods for steady-state wave scattering by interior and surface-breaking cracks with contact acoustic nonlinearity, Int. J. Solids Struct. (2020).

[34] N. Rauter, R. Lammering, A constitutive model for the analysis of second harmonic Lamb waves in unidirectional composites, Int. J. Solids Struct. 135 (2018) 184-196.

[35] Y. Shen, V. Giurgiutiu, Predictive modeling of nonlinear wave propagation for structural health monitoring with piezoelectric wafer active sensors, J. Intell. Mater. Syst. Struct. 25 (2014) 506-520.

[36] N.P. Yelve, M. Mitra, P.M. Mujumdar, Spectral damage index for estimation of breathing crack depth in an aluminum plate using nonlinear Lamb wave, Struct. Control Health Monitor. 21 (2014) 833-846.

[37] S.V. Walker, J.-Y. Kim, J. Qu, L.J. Jacobs, Fatigue damage evaluation in A36 steel using nonlinear Rayleigh surface waves, Ndt & E Int. 48 (2012) 10-15.

[38] D.T. Zeitvogel, K.H. Matlack, J.-Y. Kim, L.J. Jacobs, P.M. Singh, J. Qu, Characterization of stress corrosion cracking in carbon steel using nonlinear Rayleigh surface waves, Ndt & E Int. 62 (2014) 144-152.

[39] D. Pfeifer, J.-Y. Kim, L.J. Jacobs, Nonlinear Rayleigh waves to evaluate plasticity damage in X52 pipeline material, Mech. Syst. Sig. Process. 143 (2020) 106794.

[40] C. Yang, J.D. Achenbach, Radiation from Equivalent Body Forces for Scattering of Surface Waves by a Near-Surface Cylindrical Cavity, in: Generalized Models and Non-classical Approaches in Complex Materials 2, Springer, 2018, pp. 307-328.

[41] H. Phan, Y. Cho, J.D. Achenbach, Application of the reciprocity theorem to scattering of surface waves by a cavity, Int. J. Solids Struct. 50 (2013) 4080-4088.

[42] X. Ding, F. Li, Y. Zhao, Y. Xu, N. Hu, P. Cao, M. Deng, Generation mechanism of nonlinear Rayleigh surface waves for randomly distributed surface micro-cracks, Materials 11 (2018) 644.

[43] S. Thiele, J.-Y. Kim, J. Qu, L.J. Jacobs, Air-coupled detection of nonlinear Rayleigh surface waves to assess material nonlinearity, Ultrasonics 54 (2014) 1470-1475.

[44] J. Achenbach, Reciprocity in elastodynamics, Cambridge University Press, 2003.

[45] H. Phan, Y. Cho, J.D. Achenbach, Verification of surface wave solutions obtained by the reciprocity theorem, Ultrasonics 54 (2014) 1891-1894.

[46] M.L. Kachanov, B. Shafiro, I. Tsukrov, Handbook of elasticity solutions, Springer Science & Business Media, 2003.

[47] D. Appelö, G. Kreiss, A new absorbing layer for elastic waves, J. Comput. Phys. 215 (2006) 642-660.